

FLASHOMNI: A UNIFIED SPARSE ATTENTION ENGINE FOR DIFFUSION TRANSFORMERS

Liang Qiao^{1*} Yue Dai^{1*} Yeqi Huang² Hongyu Kan³ Jun Shi¹ Hong An¹

¹University of Science and Technology of China ²University of Edinburgh

³University of Virginia

Code: <https://github.com/qiaolian9/FlashOmni>

ABSTRACT

Multi-Modal Diffusion Transformers (DiTs) demonstrate exceptional capabilities in visual synthesis, yet their deployment remains constrained by substantial computational demands. To alleviate this bottleneck, many sparsity-based acceleration methods have been proposed. However, their diverse sparsity patterns often require customized kernels for high-performance inference, limiting universality. We propose **FlashOmni**, a unified sparse attention engine compatible with arbitrary DiT architectures. FlashOmni introduces flexible *sparse symbols* to standardize the representation of a wide range of sparsity strategies, such as feature caching and block-sparse skipping. This unified abstraction enables the execution of diverse sparse computations within a single *attention kernel*. In addition, FlashOmni designs optimized *sparse GEMMs* for attention blocks, leveraging sparse symbols to eliminate redundant computations and further improve efficiency. Experiments demonstrate that FlashOmni delivers near-linear, closely matching the sparsity ratio speedup (1:1) in attention and GEMM- Q , and achieves $2.5 \times$ – $3.8 \times$ acceleration in GEMM- O (max peaking at about 87.5% of the theoretical limit). Applied with a multi-granularity sparsity strategy, it enables the Hunyuan model (33K) to achieve about $1.5 \times$ end-to-end acceleration without degrading visual quality.

1 INTRODUCTION

Diffusion Transformers (DiTs) (Peebles & Xie, 2023) have achieved remarkable progress in high-fidelity visual generation (Esser et al., 2024; Black-Forest-Labs, 2024; Kong et al., 2024; Li et al., 2024; Batifol et al., 2025) by leveraging attention. However, its high computational complexity constrains inference efficiency, a challenge that grows with model scale, especially for high-resolution image and long video generation scenarios. To address this, various acceleration approaches have been developed, with sparsity-based methods standing out as the most universally applied techniques for their rapid, training-free deployment.

There are two distinct categories of sparse acceleration methods based on the granularity of sparsity applied during attention computation. (i) *Feature caching* (Chen et al., 2024; Selvaraju et al., 2024; Zou et al., 2024; 2025; Liu et al., 2025b) primarily exploits the feature similarity between adjacent timesteps, focusing on reusing or predicting the whole computations of selected tokens across steps to reduce the per-step computational burden by caching the corresponding feature. (ii) *Block-sparse skipping* leverages the inherent sparsity of attention computation, where many softmax operation outputs approach zero (Deng et al., 2024), to skip unimportant block-tile computations along the reduction axis via various evaluation strategies. As attention patterns vary considerably across different tasks, multiple sparse attentions have emerged, such as dynamic sparse attention (Xi et al., 2025; Zhang et al., 2025b; Xia et al., 2025; Xu et al., 2025; Yang et al., 2025) and pattern-based sparse attention (Yuan et al., 2024; Zhang et al., 2025a), each providing a task-specific sparsity design.

Despite promising progress, sparse acceleration for DiTs still faces several limitations: (i) *Inconsistent sparsity granularity*. Existing methods vary from coarse-grained caching to fine-grained block skipping. Applying a uniform strategy across all tokens often harms quality, while combining

*Equal contribution. {q1ian9, dy329261472}@mail.ustc.edu.cn

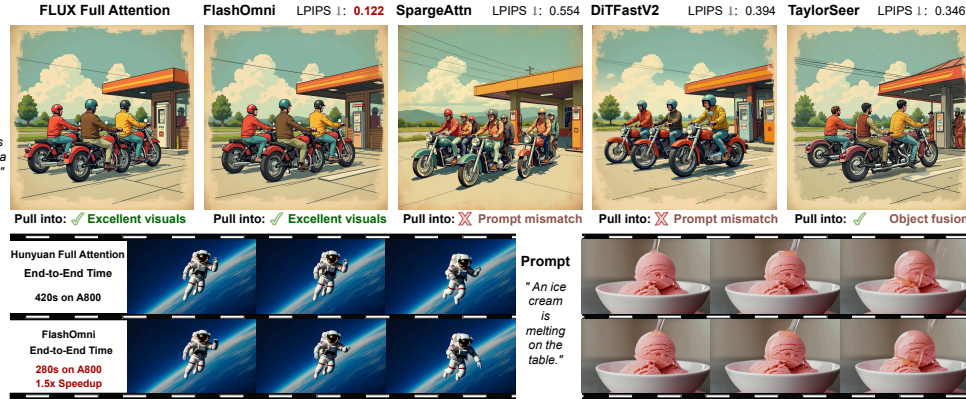


Figure 1: Visualization of different acceleration methods on FLUX and FlashOmni’s speedup on HunyuanVideo.

strategies remains difficult without a unified framework. (ii) *Fragmented design space*. Current methods introduce sparsity patterns tailored to specific tasks (e.g., dynamic vs. pattern-based attention). This fragmentation complicates the search for optimal strategies and prevents reuse across different applications. (iii) *Lack of kernel generality*. To achieve efficiency, most sparse approaches require dedicated kernels optimized for specific sparsity structures. This reduces flexibility, increases engineering overhead, and hinders scalable deployment.

To address these challenges, we propose FlashOmni, a unified sparse attention engine for diffusion transformers. FlashOmni abstracts the multi-step denoising using multi-granularity sparsity as an “*Update-Dispatch*” paradigm and introduces several key designs: (i) *Unified sparse symbols*. We introduce compact 8-bit sparse symbols to represent multiple levels of sparsity in a unified format. These symbols guide the selective update of cached features, enabling flexible multi-granularity integration. (ii) *General sparse attention kernel*. We design a single kernel that decodes sparse symbols at runtime and efficiently executes diverse sparsity strategies. This eliminates fragmentation by supporting arbitrary sparsity patterns within one engine. (iii) *Optimized sparse GEMMs*. We further develop GEMM-*Q* and GEMM-*O*, which leverage sparse symbols to eliminate redundant computations along spatial and reduction dimensions, while also improving feature-cache storage logic.

Our experiments demonstrate that our sparse kernel design achieves near-linear speedup with increasing sparsity, reaching a one-to-one acceleration with theoretical computation reduction in GEMM-*Q* and attention, up 2.5 \times to 3.8 \times acceleration in GEMM-*O* (max peaking at about 87.5% of the theoretical limit), and delivering 2 \times attention speedup with nearly 1.5 \times end-to-end gain in Hunyuan built upon FlashOmni.

Our contributions can be summarized as follows:

- We propose FlashOmni, a unified sparse attention engine for DiTs. FlashOmni enables highly efficient inference with multi-granularity sparsity by abstracting an “*Update-Dispatch*” paradigm.
- FlashOmni unifies multi-granularity sparse strategies with flexible sparse symbols and provides a general attention kernel for supporting efficient arbitrary sparse computation.
- FlashOmni designs sparse GEMMs for the attention module’s linear layer to eliminate redundant computations caused by feature caching and to improve cache storage logic.

2 RELATED WORKS

Transformers in Diffusion Models. Diffusion Transformers (Peebles & Xie, 2023), which follow scaling laws, have achieved notable success in image (Chen et al., 2024; Li et al., 2024) and video generation (Zheng et al., 2024; HaCohen et al., 2024). Recently, the Multimodal Diffusion Transformer (MMDiT), introduced by SD3 (Esser et al., 2024), offers greater advantages. It replaces the cross-attention module of DiTs by independently projecting visual inputs and text embeddings before concatenating them for self-attention. Prominent adopters include SD3 and

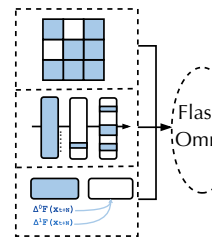


Figure 2: Typical sparse methods for DiTs.

Flux series (Black-Forest-Labs, 2024; Batifol et al., 2025) in image synthesis, and CogVideoX (Yang et al., 2024), HunyuanVideo (Sun et al., 2024), and Mochi-1 (Team, 2024) in video generation. However, iterative sampling causes significant overhead in large and complex DiTs, limiting real-time applicability. Two primary sparse acceleration strategies are detailed below and illustrated in Figure 2.

Feature Caching. Feature caching leverages representation similarity between adjacent timesteps in DiTs and can be categorized into layer-wise and token-wise strategies. approaches (Ma et al., 2024; So et al., 2024; Li et al., 2023; Wimbauer et al., 2024) mitigate redundant computation via caching, interpolation, or low-frequency updates, with extensions that cache activations in both attention and MLP layers (Chen et al., 2024; Selvaraju et al., 2024). TeaCache (Liu et al., 2025a) further refines this by dynamically estimating timestep-dependent differences, while TaylorSeer (Liu et al., 2025b) enhances generation quality by forecasting future features from historical ones. In contrast, token-wise methods target the importance of individual tokens. ToCa (Zou et al., 2025) updates cached features based on attention-derived token scores, whereas Duca (Zou et al., 2024) approximates attention weights using the norm of the value matrix to estimate token importance.

Block-Sparse Skipping. Attention computation often exhibits inherent sparsity, with many softmax outputs approaching zero—a property widely exploited in ViTs (Beltagy et al., 2020; Hassani et al., 2023; Child et al., 2019) and LLMs (Zhang et al., 2023; Xiao et al., 2023; Fu et al., 2024). Sparse attention mechanisms for accelerating DiTs can be divided into static and dynamic approaches. Static methods predefine sparse patterns offline, such as prioritizing recent tokens. DiTFastAttn (Yuan et al., 2024) combines sliding-window patterns with attention sharing, while Sparse-vDiT (Chen et al., 2025) classifies attention heads into three predefined patterns. DiTFastAttnV2 (Zhang et al., 2025a) employs Arrow Attention with caching to enable head-wise selection in MMDiT, alleviating window constraints. Dynamic methods instead construct sparsity masks at runtime. Xattention (Xu et al., 2025) uses the sum of antidiagonal values in the attention matrix to provide a powerful proxy for block importance. SpargeAttention (Zhang et al., 2025b) derives masks from QK embeddings without relying on predefined patterns, whereas SVG2 (Yang et al., 2025) uses semantic-aware permutation to capture critical tokens better and reduce redundant computation.

3 METHOD

In this section, we first outline the sparse acceleration methods for text-to-vision diffusion transformers, then introduce the FlashOmni framework (Figure 3), which incorporates novel designs across unified sparse symbols, sparse attention, and sparse GEMMs, followed by detailed descriptions.

3.1 PRELIMINARY

Text-to-vision diffusion transformers (e.g., MMDiT) experience attention bottlenecks due to concatenating fixed-length text tokens (N_{text}) with resolution-dependent visual tokens (N_{vision}), producing a joint attention map with four regions: text-to-text, $v \rightarrow t$, $t \rightarrow v$, and vision-to-vision. Standard attention computes $S = QK^\top / \sqrt{d}$, $P = \text{Softmax}(S)$, $O = PV$, with $N = N_{\text{text}} + N_{\text{vision}}$. FlashAttention (Dao, 2024) accelerates this by block-partitioning Q , K , V (sizes b_q , b_k) and applying online softmax (Milakov & Gimelshein, 2018). Acceleration strategies generally apply one sparsity pattern per block, ranging from coarse- to fine-grained:

Definition 1 (Logical Block Sparse Masks). $M_c \in \{0, 1\}^{\lceil N/b_q \rceil}$ marks cached output blocks; $M_s \in \{0, 1\}^{\lceil N/b_q \rceil \times \lceil N/b_k \rceil}$ marks skipped $Q_i K_j^\top$ and $P_{ij} V_j$ computations.

Definition 2 (Sparse Strategies). Feature caching reuses O_i when $M_c[i] = 0$, refreshing masks and cache at *Update* steps. Block-sparse skipping omits pairs with $M_s[i, j] = 0$, with dynamic masks updated from the latest Q , K , and static masks pre-tuned offline for zero update cost.

3.2 FLASHOMNI OVERVIEW

Figure 4 presents the operational flow of FlashOmni, which adopts an “*Update-Dispatch*” framework to integrate and execute two sparsity strategies across two primary phases:

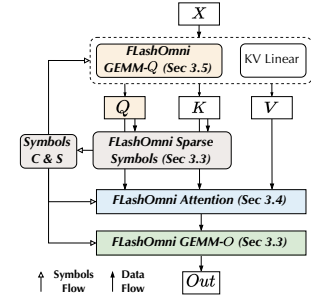


Figure 3: FlashOmni design.

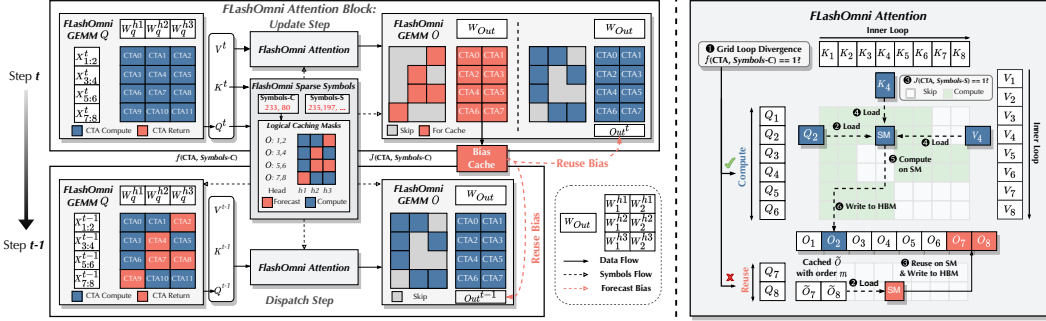


Figure 4: Detailed workflow of the FlashOmni framework: incorporating unified sparse symbols and sparse kernels (general sparse attention and GEMMs). Unified sparse symbols are refreshed only at *Update* timesteps, providing sparse guidance for corresponding sparse kernel executions at *Dispatch* timesteps.

Update: Given a sequence of adjacent timesteps $\{t, t-1, \dots, t-\mathcal{N}\}$, FlashOmni first refreshes the sparse symbols and feature cache at the current step t . Using the newly computed Q and K , a tailored sparsity-selection policy determines the sparsity type for each token block in the upcoming steps. Full attention is then applied to update the feature cache. When an output projection is present, FlashOmni additionally leverages GEMM- O to optimize cache updates further.

Dispatch: Utilizing the sparse symbols produced in the Update phase, FlashOmni accelerates attention computation over the following \mathcal{N} timesteps $\{t-1, \dots, t-\mathcal{N}\}$. Within the attention module, Cooperative Thread Arrays (CTA) adopt specialized computation modes, enabling different sparsity granularities for their respective block tiles. Guided by the caching symbols, FlashOmni also applies GEMM- Q and GEMM- O optimizations, removing redundant operations.

3.3 FLASHOMNI SPARSE SYMBOLS

FlashOmni employs two sparse symbols, \mathcal{S}_c and \mathcal{S}_s , serving as a unified representation for multiple sparsity approaches, including feature caching and block-sparse skipping. Using MMDiT as a case study, we examine the joint attention map to determine the applicability of sparsity at two distinct granularities and derive the combination strategy adopted in FlashOmni.

Observation 1. In text-to-vision diffusion transformers, the $v \rightarrow t$ and $t \rightarrow v$ regions of the attention map are essential for reliable multimodal fusion. At each timestep, $v \rightarrow t$ updates text tokens via $P_{v \rightarrow t} V_{\text{vision}}$, embedding visual context into O_{text} . Conversely, $t \rightarrow v$ updates vision tokens via $P_{t \rightarrow v} V_{\text{text}}$, injecting textual guidance into O_{vision} . These two interactions are complementary: omitting $v \rightarrow t$ prevents text from perceiving visual changes, whereas omitting $t \rightarrow v$ leads to vision outputs misaligned with textual prompts. Empirically, we observe that caching image tokens that significantly influence text tokens, or are strongly affected by control-signal tokens, degrades cross-modal consistency. Therefore, FlashOmni excludes such tokens from caching to ensure timely and accurate multimodal updates.

Logical Masks Generation. FlashOmni first infers sparsity patterns from the attention structure and encodes them into logical block-sparse masks. These patterns are derived from a compressed attention map, which serves as the basis for constructing the sparse strategy combination used in this work. Specifically, every n consecutive $\{Q_i\}$ and $\{K_j\}$ blocks (e.g., two blocks in Figure 4) are aggregated into single tokens q and k through token-gathering operations such as mean pooling, with pooling sizes b_q and b_k . The compressed tokens $\{q_i\}$ and $\{k_j\}$ form a reduced attention map $\tilde{S} = \text{Softmax}(\tilde{S})$, where $\tilde{S} = \{q_i\}\{k_j^T\} \in \mathbb{R}^{[N/(nb_q)] \times [N/(nb_k)]}$. From this representation, we define two metrics for guiding feature caching: (i) Vision-to-Text Contribution ($\mathcal{C}_{i, v \rightarrow t}$): for vision block i , this measures its contribution to text blocks based on the compressed attention map. Lower values indicate less influence on text tokens and are therefore prioritized for caching. Denoting $\alpha_{i,j}$ as the (i, j)

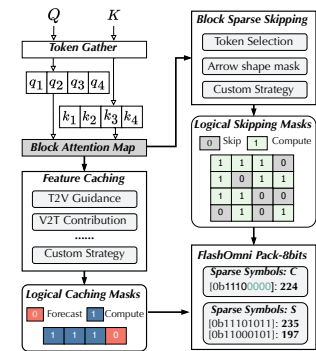


Figure 5: Example of FlashOmni sparse symbols generation for a single head of attention.

element in $\tilde{P}[:, n_t, n_t :]$, where $n_t = \lceil n_t / (nb_q) \rceil$ is the number of compressed text blocks, the metric is computed as $\mathcal{C}_{i,v \rightarrow t} = \sum_{j=1}^{n_t} \alpha_{j,i}$. (ii) Text-to-Vision Guidance ($\mathcal{G}_{i,t \rightarrow v}$): this reflects the extent to which vision block i is influenced by text blocks. Blocks under stronger textual guidance retain attention computation to preserve responsiveness. With $\beta_{i,j}$ denoting the (i, j) element in $\text{Softmax}(\tilde{P}[n_t :, : n_t]^T)$, the score is given by $\mathcal{G}_{i,t \rightarrow v} = \sum_{j=1}^{n_t} \beta_{j,i}$. Given $\mathcal{C}_{i,t \rightarrow v}$ and $\mathcal{G}_{i,v \rightarrow t}$, FlashOmni selects the indices with the lowest combined scores such that their cumulative sums do not exceed thresholds $\tau_c \cdot \sum_i \mathcal{C}_{i,t \rightarrow v}$ and $\tau_c \cdot \sum_i \mathcal{G}_{i,v \rightarrow t}$, as formalized in Equation 1:

$$\{ i \mid \text{CumSum}_{\uparrow}(\mathcal{C}_{i,t \rightarrow v}) \leq \tau_c \cdot \sum_j \mathcal{C}_{j,t \rightarrow v} \wedge \text{CumSum}_{\uparrow}(\mathcal{G}_{i,v \rightarrow t}) \leq \tau_c \cdot \sum_j \mathcal{G}_{j,v \rightarrow t} \} \quad (1)$$

Blocks with minimal scores are cached for use in the next step, while others undergo full attention computation. In the logical caching mask $M_c[i]$, cached positions are assigned 0 and non-cached positions 1. For cached blocks, FlashOmni employs TaylorSeer (Liu et al., 2025b) to forecast future features via Taylor series expansion using stored features and their derivatives. For block-sparse skipping, token selection follows the compressed attention map, aligning with the approach of SpargeAttn (Zhang et al., 2025b).

Sparse Symbols Compression. To reduce storage overhead, the logical masks are encoded as 8-bit compressed sparse symbols: \mathcal{S}_c for feature caching and \mathcal{S}_s for block-sparse skipping, as shown in Figure 5. In each *Update* step, the latest Q and K are block-aggregated to form the attention map, from which masks are generated via the two-granularity sparsity strategy. For example, $M_c[4] = 0$ skips the computation of O_7 and O_8 and reusing previous O_7 and O_8 during the "Dispatch" step. With big-end alignment, zero-padding yields the binary 0b11100000, stored as the uint8 224 for \mathcal{S}_c ; \mathcal{S}_s can similarly be encoded as 235 and 197.

3.4 FLASHOMNI ATTENTION

Following the generation of sparse symbols \mathcal{S}_c and \mathcal{S}_s , the objective of FlashOmni is to implement a general attention kernel that can interpret these symbols and execute arbitrary sparse computations efficiently. In the conventional FlashAttention framework, each CTA processes a complete computation tile. To support sparsity, we extend this design so that each CTA can detect and adapt to different sparsity patterns, as outlined in Algorithm 1. Specifically, before loading Q_i , each CTA invokes the spatial-axis decoding function \mathcal{F} (Line 5) and checks \mathcal{S}_c to determine whether the current tile requires computation. Depending on this result, execution follows either a compute-on-demand or a cache-then-reuse path. The decoding operation uses only bitwise procedures, expressed as $\mathcal{F}(\mathcal{S}_c, i) = (\mathcal{S}_c >> i/n) \& 1$.

In the cache-then-reuse path, element-wise computation logic is fused into the FlashOmni attention process, allowing each CTA to choose between standard attention or lightweight element-wise operations (e.g., summation and multiplication in TaylorSeer) based on the decoding result. Alternatively, an elementwise kernel can be invoked to perform simple value-reuse computations and write the results into the output tensor O . The corresponding CTA of feature caching can then directly return (Line 7) without further processing. In the compute-on-demand path, an additional reduction-axis decoding function \mathcal{J} (Line 13) is applied before updating $O_{i,j}$ in the inner loop to determine whether to skip specific blocks by decoding \mathcal{S}_s . This operation is defined as $\mathcal{J}(\mathcal{S}_s, i, j) = (\mathcal{S}_s >> \frac{i}{n} \frac{T_{kv}}{n} + \frac{j}{n}) \& 1$. Directly performing this bitwise operation for every K_j load increases CUDA core overhead. To mitigate this, undecoded bits are processed only once when first encountered, and the results—covering up to $8n$ consecutive blocks—are stored in registers for subsequent reuse.

Algorithm 1: FlashOmni Attention

Input:
1 $\{Q_i\} \in \mathbb{R}^{T_q \times b_q \times d}; T_q = N/b_q$
2 $\{K_i\}, \{V_i\} \in \mathbb{R}^{T_{kv} \times b_k \times d}; T_{kv} = N/b_k$
3 **Sparse symbols:** $\mathcal{S}_c, \mathcal{S}_s$; **Cached output:** \tilde{O} ;
Output: O
4 **for** $i \leftarrow 1$ **to** T_Q
5 **if** $\mathcal{F}(\mathcal{S}_c, i) == 0$ **then**
6 **# Cache-then-Reuse.**
7 **Continue if** O_i **is already updated;**
8 Load \tilde{O}_i **into the SM**;
9 $O_i = \text{OP}_{\text{reuse}}(\tilde{O}_i);$
10 **else**
11 Load O_i^t **into the SM**;
12 **for** $j \leftarrow 1$ **to** T_{kv}
13 **if** $\mathcal{J}(\mathcal{S}_s, i, j) == 1$ **then**
14 **# Compute-on-Demand.**
15 Load K_j, V_j ;
16 $Q_i K_j^T$;
17 Update $m_{i,j}, \tilde{P}_{ij}, l_{i,j}$;
18 $\tilde{P}_{ij} V_j \rightarrow O_{i,j}$;
19 $O_i = \text{diag}(l_{i,T_n})^{-1} O_{i,T_n}$
20 Write O_i **into HBM**;
21 **return** $O = \{O_i\}$;

3.5 FLASHOMNI SPARSE GEMMS

FlashOmni introduces two *sparse GEMMs*, GEMM-*Q* and GEMM-*O*, utilizing \mathcal{S}_c to remove redundant computations in the Linear layers: query projection ($\text{Proj}_{\text{to_q}}$) and output projection ($\text{Proj}_{\text{to_out}}$) within attention modules.

Observation 2. In typical attention modules of common DiT architectures, the computation from the input tensor X to the final attention output O involves three main stages: (1) generating the query vectors Q from X ; (2) using Q to compute attention scores with the corresponding keys and aggregating the values; and (3) writing the aggregated results into the output tensor O . Specifically, the generation of Q from X typically consists of three sequential operations: query projection ($\text{Proj}_{\text{to_q}}$), token-wise RMS normalization ($\text{OP}_{\text{RMSNorm}}$), and rotary positional encoding (OP_{RoPE}). The standard attention output formulation $O_i^h = \sum_j P_{i,j}^h V_j^h$ can be expanded as Equation 2.

$$O_i^h = \sum_j \text{Softmax} \left(\frac{\text{OP}_{\text{RoPE}}(\text{OP}_{\text{RMSNorm}}(X_i W_{\text{to_q}}^h)) (K^h)^T}{\sqrt{d}} \right)_j V_j^h \quad (2)$$

Both RMSNorm and RoPE operate exclusively along the feature dimension for each token, without cross-token computation. Therefore, at the *Dispatch* step, if \mathcal{S}_c specifies that a particular block O_i^h is retrieved from the cache \tilde{O}_i^h , the corresponding query projection $Q_i^h = X_i W_{\text{to_q}}^h$ can be skipped.

FlashOmni GEMM-Q. As shown in the left part of Figure 4 (FlashOmni GEMM-*Q*), newly computed Q values are required to refresh the symbol information at the *Update* step, and the GEMM-*Q* operation will follow its full-standard execution. At the *Dispatch* step, each CTA applies the spatial-axis decoding function \mathcal{F} to \mathcal{S}_c to determine whether its block tile participates in the upcoming attention computation. If not, the CTA exits immediately without performing any further operations.

Observation 3. In typical DiT architectures, once the attention output for each head, O_i^h , is obtained, an output projection ($\text{Proj}_{\text{to_out}}$) is usually applied to facilitate information exchange across heads for the same token, which can be expressed as Equation 3, where the set $H_i = \{h \mid J(\mathcal{S}_c, i, h) = 1\}$ denotes the heads whose attention outputs are generated directly by attention computation at the current step, rather than obtained via feature caching.

$$\text{Out}_i = \sum_h O_i^h W_{\text{to_out}}^h = (\sum_{h \notin H_i} + \sum_{h \in H_i}) O_i^h W_{\text{to_out}}^h \quad (3)$$

At the *Dispatch* step, when \mathcal{S}_c specifies that the output features of head h for block i are retrieved from cache \tilde{O}_i^h , the operation can be expressed as $O_i^h = \text{OP}_{\text{reuse}}(\tilde{O}_i^h)$ for $h \notin H_i$. Since OP_{reuse} is an element-wise operation, the following property holds:

$$\sum_{h \notin H_i} O_i^h W_{\text{to_out}}^h = \sum_{h \notin H_i} \text{OP}_{\text{reuse}}(\tilde{O}_i^h) W_{\text{to_out}}^h = \text{OP}_{\text{reuse}}(\sum_{h \notin H_i} \tilde{O}_i^h W_{\text{to_out}}^h). \quad (4)$$

This property enables caching of $\sum_{h \notin H_i} \tilde{O}_i^h W_{\text{to_out}}^h$ as a bias term \mathcal{B}_c at the *Update* step. At later *Dispatch* steps, the cached bias can be transformed using an element-wise kernel, $\text{OP}_{\text{reuse}}(\mathcal{B}_c)$, and added directly to remaining computations of $\text{Proj}_{\text{to_out}}$ ($\sum_{h \in H_i} O_i^h W_{\text{to_out}}^h$) as a bias. This design eliminates redundant reduction-axis computations in the GEMM kernel. Furthermore, storing the cache bias removes the need to retain \tilde{O}_i^h in HBM at *Update* steps. The related element-wise operations in FlashOmni Attention can also be skipped entirely, allowing the cache-then-reuse branch to terminate immediately. This design reduces both computational cost and memory consumption.

FlashOmni GEMM-O. As illustrated in the right part of Figure 4 (FlashOmni GEMM-*O*), the GEMM-*O* computation is divided into two stages. For each block tile O_i^h along the reduction axis, each CTA applies the reduction-axis decoding function \mathcal{J} on \mathcal{S}_c to determine whether the tile should be generated via cache-and-reuse or computed on demand. At the *Update* step, the latest \mathcal{S}_c and attention outputs O are generated, and the cache bias \mathcal{B}_c is subsequently refreshed. In the first stage, CTAs identify tiles that will be reused at the *Dispatch* step, compute their outputs, and record the results in \mathcal{B}_c . The second stage then relaunches the kernel, processing the remaining tiles that are always updated through attention computations at the next future steps and adding the cached bias. At the *Dispatch* step, the GEMM-*O* output space is initialized via OP_{reuse} , executing only the computations corresponding to the second stage of the *Update* step. This strategy eliminates redundant operations on cached tiles, thereby reducing both computational workload and memory usage.

Table 1: End-to-end metrics comparison with block-sparse skipping across image and video generation models.

Method(seq_len) FLUX.1(4.5K)	Configuration	TOPS (\uparrow)	Sparsity (% , \uparrow)	PSNR (\uparrow)	LPIPS (\downarrow)	SSIM \uparrow	CLIP-IQA (\uparrow)	FID (\downarrow)
Full-Attention	[dev]: 50 steps 50% steps	93.82	0 50	∞ 16.69	— 0.3426	— 0.7004	0.5154 0.5054	— 56.589
DiTFastAttnV2	($\theta = 0.2$)	114.25	26	20.289	0.2174	0.7901	0.5037	39.436
SpurgeAttn	($l_1 = 6.5\%$, $l_2 = 7\%$)	101.41	22	21.358	0.1868	0.8148	0.5072	34.156
Dyn-Sparse	(5%, 15%, 4, 0, 0%)	133.12	31	24.259	0.1209	0.8665	0.5129	25.163
FlashOmni	(5%, 15%, 4, 0, 0%)	119.35	28	24.563	0.1154	0.8716	0.5124	23.942
FlashOmni	(50%, 15%, 4, 1, 0%)	149.25	41	25.159	0.0992	0.8838	0.5126	20.933
FlashOmni	(50%, 15%, 5, 1, 0%)	152.25	43	23.994	0.1241	0.8618	0.5165	25.594
FlashOmni	(50%, 15%, 5, 2, 30%)	163.19	46	23.859	0.1281	0.8575	0.5123	25.997

Method(seq_len) Hunyuan Video (33K)	TOPS (\uparrow)	Sparsity(\uparrow)	PSNR (\uparrow)	LPIPS (\downarrow)	SSIM (\uparrow)	Smoothness (\uparrow)	Consistency (\uparrow)	Flickering (\uparrow)	Style (\uparrow)
Full-Attention (50 steps)	92.32	0	∞	—	—	99.33	97.87	99.221	0.2394
DiTFastAttnV2 ($\theta = 0.2$)	124.83	31	19.751	0.3086	0.7331	99.13	97.44	99.098	0.2381
SpurgeAttn ($l_1 = 6\%$, $l_2 = 6.5\%$)	110.54	32	21.701	0.2442	0.7748	99.21	97.42	98.993	0.2399
FlashOmni (40%, 1%, 3, 1, 0)	135.93	34	32.192	0.0571	0.9289	99.32	97.69	99.217	0.2401
FlashOmni (40%, 1%, 6, 1, 0)	149.85	39	28.733	0.0946	0.8918	99.29	97.55	99.198	0.2401
FlashOmni (50%, 5%, 6, 1, 30%)	173.12	47	27.877	0.1195	0.8699	99.33	97.55	99.224	0.2392

4 EXPERIMENTS

4.1 SETUP

Models. Our experiments are performed on three SOTA visual generative models: the text-to-image generator FLUX.1-dev (Black-Forest-Labs, 2024), the text-to-video generator HunyuanVideo (Kong et al., 2024), and the text-guided image editing model FLUX.1-Kontext (Batifol et al., 2025).

Benchmarks and Metrics. For the text-to-image generation experiments, we conduct inference on the COCO-2017 dataset (Lin et al., 2014) at a resolution of 1024×1024 pixels. The text-guided image editing evaluation is performed on KontextBench (Batifol et al., 2025), which contains 1,026 unique image–prompt pairs derived from 108 base images. Generated outputs are assessed using CLIP-IQA (Wang et al., 2023) and FID-FP16 (Heusel et al., 2017), measuring image quality and distributional similarity, respectively. For text-to-video generation, we adopt VBench (Huang et al., 2024) to evaluate various aspects of video quality, including background consistency, motion smoothness, temporal flicker, and stylistic coherence. Fidelity to the original results is quantified using PSNR, SSIM (Wang et al., 2004), and LPIPS (Zhang et al., 2018).

To measure computational efficiency of sparse attention, we report TOPS (tera-operations per second), defined as attn/t , and **Sparsity**, defined as $(\text{skip}/\text{total})$ following SpurgeAttn (Zhang et al., 2025b). Here, attn denotes the total number of operations in a standard attention computation, t is the latency from given (Q, K, V) inputs to the corresponding attention outputs, skip is the number of skipped attention pairs $(Q_i K_j^\top, \tilde{P}_{ij} V_j)$, and total is the total number of such pairs.

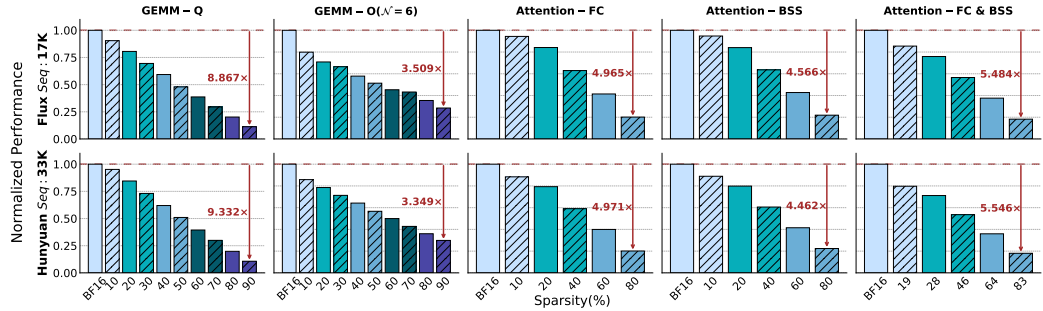
Baselines and Platform. We compare FlashOmni with five SOTA baselines: two block-sparse attention skipping methods: SpurgeAttn (Zhang et al., 2025b) and DiTFastAttnV2 (Zhang et al., 2025a), and three feature caching methods: ToCa (Zou et al., 2025), FORA (Selvaraju et al., 2024), and TaylorSeer (Liu et al., 2025b). The configuration for FlashOmni is specified as $(\tau_q, \tau_{kv}, \mathcal{N}, \mathcal{D}, S_q)$ (Appendix A.1.1). All experiments are executed on a single NVIDIA A100 GPU.

4.2 VISUAL QUALITY EVALUATION

As shown in Table 1 and Table 2, FlashOmni consistently outperforms all baselines across quality metrics on FLUX and HunyuanVideo. Compared with block-sparse skipping (DiTFastAttnV2, SpurgeAttn), it achieves higher sparsity under various threshold settings while maintaining clearly superior quality. Against caching methods (FORA, ToCa, TaylorSeer), FlashOmni attains better quality on FLUX under the same moderate cache interval ($\mathcal{N} = 5$) and order \mathcal{D} . Even under the more aggressive interval ($\mathcal{N} = 6$), FlashOmni maintains substantial advantages on both FLUX ($1.74 \uparrow$ SSIM over TaylorSeer) and HunyuanVideo ($2.97 \uparrow$ SSIM over TaylorSeer). Similar performance gains are also observed on FLUX.1-Kontext (Table 5), where FlashOmni surpasses all other methods.

Table 2: End-to-end metrics comparison with feature caching across image and video generation models.

Method(seq_len) FLUX.1(4.5K)	Configuration	PSNR (\uparrow)	LPIPS (\downarrow)	SSIM \uparrow	CLIP-IQA (\uparrow)	FID (\downarrow)		
Full-Attention	[dev]: 50 steps 50% steps	∞ 16.69	— 0.3426	— 0.7004	0.5154 0.5054	— 56.589		
FORA	($\mathcal{N} = 5$)	22.846	0.1595	0.825	0.5111	31.188		
ToCa	($\mathcal{N} = 5$)	22.827	0.2059	0.7978	0.5095	29.947		
TaylorSeer	($\mathcal{N} = 5, \mathcal{D} = 1$)	22.852	0.1441	0.8361	0.5103	28.253		
TaylorSeer	($\mathcal{N} = 5, \mathcal{D} = 2$)	23.177	0.1402	0.8395	0.5131	27.376		
FlashOmni	(50%, 15%, 5, 0, 30%)	23.355	0.1452	0.8452	0.5159	28.925		
FlashOmni	(50%, 15%, 5, 1, 30%)	23.866	0.1283	0.8575	0.5119	25.994		
FlashOmni	(50%, 15%, 5, 2, 30%)	23.859	0.1281	0.8575	0.5123	25.997		
FlashOmni	(50%, 15%, 5, 1, 0%)	23.994	0.1241	0.8618	0.5165	25.594		
TaylorSeer	($\mathcal{N} = 6, \mathcal{D} = 2$)	22.245	0.1615	0.8199	0.5119	31.082		
FlashOmni	(50%, 15%, 6, 1, 30%)	23.217	0.1507	0.8373	0.5124	28.965		
Method(seq_len) Hunyuan Video (33K)		PSNR (\uparrow)	LPIPS (\downarrow)	SSIM (\uparrow)	Smoothness (\uparrow)	Consistency (\uparrow)	Flickering (\uparrow)	Style (\uparrow)
Full-Attention (50 steps)		∞	—	—	99.33	97.87	99.221	0.2394
TaylorSeer ($\mathcal{N} = 6, \mathcal{D} = 1$)		26.483	0.1229	0.8621	99.32	97.38	99.196	0.2388
FlashOmni (50%, 5%, 6, 1, 30%)		27.877	0.1195	0.8699	99.33	97.55	99.224	0.2392
FlashOmni (40%, 1%, 6, 1, 0)		28.733	0.0946	0.8918	99.29	97.55	99.198	0.2401

Figure 6: Normalized inference performance on NVIDIA A100 (BF16, measured by using cudaLib and FlashInfer) at different sparsity levels for sparse GEMM-Q/O ($\mathcal{N} = 6$) and Attention kernels. FC and BSS indicate the application of feature caching and block-sparse skipping, respectively.

4.3 EFFICIENCY EVALUATION

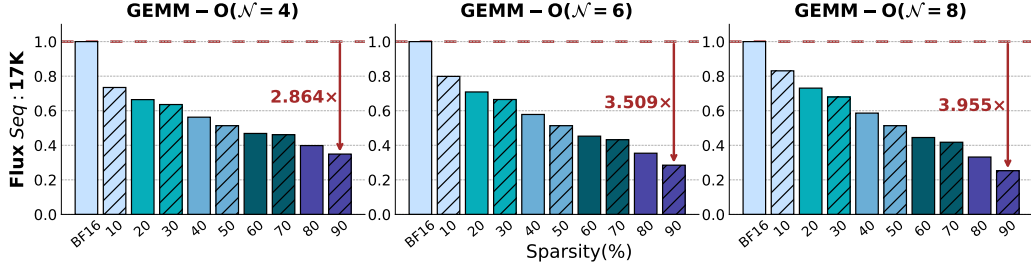
Attention performance. We implement our sparse attention kernel based on FlashInfer (Ye et al., 2025), designed to remove computations deemed unnecessary by sparse symbols dynamically. We evaluate its performance through a systematic comparison with relevant baselines using randomly generated sparse symbols under three configurations: (1) feature caching (FC) only, (2) block-sparse skipping (BSS) only, and (3) both enabled. For each configuration, we report speedup across varying sparsity ratios and compare it with the theoretical computation reduction. The right three columns in Figure 6 show that the empirical speedup closely matches the theoretical prediction and scales linearly with sparsity. More detailed experimental results are provided in the Appendix A.2.

At the same sparsity level, FC consistently yields higher performance than BSS. For instance, at 80% sparsity, FC achieves a $4.97 \times$ speedup, while BSS reaches $4.6 \times$. This difference arises because FC requires decoding only once per CTA, whereas BSS performs decoding repeatedly throughout the reduction process, incurring additional CUDA core overhead. For video generation, as shown in Figure 1, FlashOmni delivers up to $1.5 \times$ end-to-end acceleration under a 46% sparsity setting.

Sparse GEMMs performance. We also implement our sparse GEMM kernels based on CuTe to mitigate redundant computation and memory overhead introduced by enabling the FC strategy in attention. We conduct extensive experiments on both the GEMM-Q/O, observing a consistent linear speedup trend with increasing sparsity. For GEMM-Q, acceleration occurs along the spatial axis. Since decoding is performed only once, the achieved speedup closely matches the theoretical upper bound of computation reduction. For GEMM-O, sparsity lies along the reduction axis, requiring

Table 3: The ablation study evaluates FlashOmni with different configurations on FLUX.1.

Configuration	PSNR (\uparrow)	LPIPS (\downarrow)	SSIM (\uparrow)	FID (\downarrow)
(5%, 15%, $\mathcal{N} = 3$, 1, 0)	26.702	0.0784	0.9041	16.495
(5%, 15%, $\mathcal{N} = 4$, 1, 0)	25.217	0.0999	0.8837	20.789
(5%, 15%, $\mathcal{N} = 5$, 1, 0)	24.193	0.1214	0.8650	24.860
(5%, 15%, $\mathcal{N} = 6$, 1, 0)	23.454	0.1366	0.8506	28.072
(5%, 15%, $\mathcal{N} = 7$, 1, 0)	23.012	0.1488	0.8405	30.541
(50%, 15%, 5, $\mathcal{D} = 0$, 30%)	23.355	0.1452	0.8452	28.925
(50%, 15%, 5, $\mathcal{D} = 1$, 30%)	23.866	0.1283	0.8575	25.994
(50%, 15%, 5, $\mathcal{D} = 2$, 30%)	23.859	0.1281	0.8575	25.997

Figure 8: Normalized inference performance at different \mathcal{N} for sparse GEMM- O , where token length is 17K.

multiple decoding operations, preventing a one-to-one match with the theoretical peak speedup; nevertheless, the achieved performance remains close. For instance, at 90% sparsity with $\mathcal{N} = 6$, the theoretical speedup is $4 \times$ (speedup analysis refers to Appendix A.1.2), while our kernel attains $3.3 \times \sim 3.5 \times$ (Figure 6). This discrepancy arises because GEMM- O requires multiple decoding operations along the reduction axis on CUDA cores. As for a single inference, even at 90% sparsity, while GEMM- Q alone can achieve a near-linear $9 \times$ speedup, GEMM- O only reaches $6.39 \times$ due to these additional overheads. More details refer to the Appendix A.3.

Density analysis. We further measure the computation density during inference on HunyuanVideo, as illustrated in Figure 7. For SpargeAttn, the density remains relatively stable throughout the inference process. In contrast, FlashOmni exhibits a sharp drop in density from an initial value close to 1, maintaining overall lower density both at the whole-model level and within individual transformer layers. We attribute FlashOmni’s ability to achieve higher video generation quality despite lower density to the critical role of the early denoising steps in the DiT inference process.

In these initial stages, the vision token is randomly initialized from Gaussian noise and requires strong and comprehensive text guidance, alongside timely updates of the textual signal, consistent with our findings in Observation 1. Moreover, under our degradation strategy, when the proportion of token blocks requiring updates falls below a certain threshold, we directly employ full-feature caching to improve efficiency, whose details refer to Appendix A.1.1.

4.4 ABLATION STUDY

We perform ablation experiments (Table 3) on Flux to assess how the interval \mathcal{N} and caching order \mathcal{D} affect generation quality. First-order caching ($\mathcal{O} = 1$) delivers the largest performance gains, while higher orders degrade quality, highlighting the limits of simulation in capturing real-world behavior. Despite its bias, first-order caching remains more faithful than direct reuse. Increasing \mathcal{N} offers greater acceleration but at the cost of noticeable quality loss.

We further conduct ablation experiments (Figure 8) to evaluate the speedup of GEMM- O across settings \mathcal{N} with a sequence length of 17K. As \mathcal{N} increases, the overall speedup consistently improves but falls short of the theoretical speedup predicted by reduced FLOPs. For example, when $\mathcal{N} = 4, 6, 8$, the measured 93.1%, 87.7%, and 84.7% of theoretical speedup, respectively. This discrepancy arises

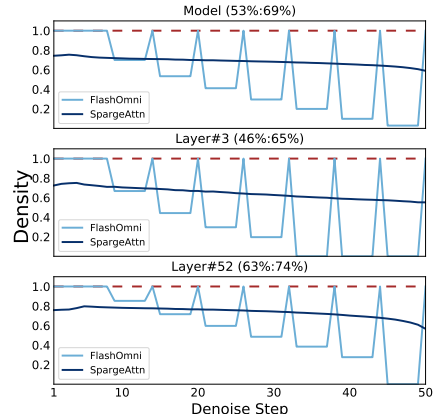


Figure 7: Density comparison with SpargeAttn on HunyuanVideo benchmark.

because GEMM- O requires multiple decoding operations along the reduction axis on CUDA cores; even at 90% sparsity, while GEMM- Q alone can achieve a near-linear $9\times$ speedup, GEMM- O only reaches $6.39\times$ due to these additional overheads. As \mathcal{N} grows, this effect becomes increasingly pronounced in the aggregated GEMM- O speedup.

5 CONCLUSION

We propose FlashOmni, a unified sparse attention engine that is applicable to any Diffusion Transformers. FlashOmni abstracts an *Update-Dispatch* paradigm with three key designs: it unifies multi-granularity spare strategies with flexible sparse symbols, supports efficient arbitrary sparse attention through a general kernel, and optimizes sparse GEMMs in attention linear layers to remove redundant computation. Experiments demonstrate that FlashOmni achieves significant end-to-end acceleration across diverse models without retraining, while preserving generation quality.

REFERENCES

Stephen Batifol, Andreas Blattmann, Frederic Boesel, Saksham Consul, Cyril Diagne, Tim Dockhorn, Jack English, Zion English, Patrick Esser, Sumith Kulal, et al. Flux. 1 kontext: Flow matching for in-context image generation and editing in latent space. *arXiv e-prints*, pp. arXiv-2506, 2025. [1](#), [3](#), [7](#)

Iz Beltagy, Matthew E Peters, and Arman Cohan. Longformer: The long-document transformer. *arXiv preprint arXiv:2004.05150*, 2020. [3](#)

Black-Forest-Labs. Flux.1, 2024. URL <https://blackforestlabs.ai/>. [1](#), [3](#), [7](#)

Pengtao Chen, Mingzhu Shen, Peng Ye, Jianjian Cao, Chongjun Tu, Christos-Savvas Bouganis, Yiren Zhao, and Tao Chen. δ -dit: A training-free acceleration method tailored for diffusion transformers. *arXiv preprint arXiv:2406.01125*, 2024. [1](#), [2](#), [3](#)

Pengtao Chen, Xianfang Zeng, Maosen Zhao, Peng Ye, Mingzhu Shen, Wei Cheng, Gang Yu, and Tao Chen. Sparse-vdit: Unleashing the power of sparse attention to accelerate video diffusion transformers. *arXiv preprint arXiv:2506.03065*, 2025. [3](#)

Rewon Child, Scott Gray, Alec Radford, and Ilya Sutskever. Generating long sequences with sparse transformers. *arXiv preprint arXiv:1904.10509*, 2019. [3](#)

Tri Dao. Flashattention-2: Faster attention with better parallelism and work partitioning. In *The Twelfth International Conference on Learning Representations*, 2024. [3](#)

Yichuan Deng, Zhao Song, and Chiwun Yang. Attention is naturally sparse with gaussian distributed input. *CoRR*, 2024. [1](#)

Patrick Esser, Sumith Kulal, Andreas Blattmann, Rahim Entezari, Jonas Müller, Harry Saini, Yam Levi, Dominik Lorenz, Axel Sauer, Frederic Boesel, et al. Scaling rectified flow transformers for high-resolution image synthesis. In *Forty-first international conference on machine learning*, 2024. [1](#), [2](#)

Tianyu Fu, Haofeng Huang, Xuefei Ning, Genghan Zhang, Boju Chen, Tianqi Wu, Hongyi Wang, Zixiao Huang, Shiyao Li, Shengen Yan, et al. Moa: Mixture of sparse attention for automatic large language model compression. *arXiv preprint arXiv:2406.14909*, 2024. [3](#)

Yoav HaCohen, Nisan Chiprut, Benny Brazowski, Daniel Shalem, Dudu Moshe, Eitan Richardson, Eran Levin, Guy Shiran, Nir Zabari, Ori Gordon, et al. Ltx-video: Realtime video latent diffusion. *arXiv preprint arXiv:2501.00103*, 2024. [2](#)

Ali Hassani, Steven Walton, Jiachen Li, Shen Li, and Humphrey Shi. Neighborhood attention transformer. In *Proceedings of the IEEE/CVF conference on computer vision and pattern recognition*, pp. 6185–6194, 2023. [3](#)

Martin Heusel, Hubert Ramsauer, Thomas Unterthiner, Bernhard Nessler, and Sepp Hochreiter. Gans trained by a two time-scale update rule converge to a local nash equilibrium. *Advances in neural information processing systems*, 30, 2017. 7

Ziqi Huang, Yinan He, Jiashuo Yu, Fan Zhang, Chenyang Si, Yuming Jiang, Yuanhan Zhang, Tianxing Wu, Qingyang Jin, Nattapol Chanpaisit, et al. Vbench: Comprehensive benchmark suite for video generative models. In *Proceedings of the IEEE/CVF Conference on Computer Vision and Pattern Recognition*, pp. 21807–21818, 2024. 7

Weijie Kong, Qi Tian, Zijian Zhang, Rox Min, Zuozhuo Dai, Jin Zhou, Jiangfeng Xiong, Xin Li, Bo Wu, Jianwei Zhang, et al. Hunyuanvideo: A systematic framework for large video generative models. *arXiv preprint arXiv:2412.03603*, 2024. 1, 7

Senmao Li, Taihang Hu, Fahad Shahbaz Khan, Linxuan Li, Shiqi Yang, Yaxing Wang, Ming-Ming Cheng, and Jian Yang. Faster diffusion: Rethinking the role of unet encoder in diffusion models. *CoRR*, 2023. 3

Zhimin Li, Jianwei Zhang, Qin Lin, Jiangfeng Xiong, Yanxin Long, Xinchi Deng, Yingfang Zhang, Xingchao Liu, Minbin Huang, Zedong Xiao, et al. Hunyuan-dit: A powerful multi-resolution diffusion transformer with fine-grained chinese understanding. *arXiv preprint arXiv:2405.08748*, 2024. 1, 2

Tsung-Yi Lin, Michael Maire, Serge Belongie, James Hays, Pietro Perona, Deva Ramanan, Piotr Dollár, and C Lawrence Zitnick. Microsoft coco: Common objects in context. In *European conference on computer vision*, pp. 740–755. Springer, 2014. 7

Feng Liu, Shiwei Zhang, Xiaofeng Wang, Yujie Wei, Haonan Qiu, Yuzhong Zhao, Yingya Zhang, Qixiang Ye, and Fang Wan. Timestep embedding tells: It’s time to cache for video diffusion model. In *Proceedings of the Computer Vision and Pattern Recognition Conference*, pp. 7353–7363, 2025a. 3

Jiacheng Liu, Chang Zou, Yuanhuiyi Lyu, Junjie Chen, and Linfeng Zhang. From reusing to forecasting: Accelerating diffusion models with taylorseers. *arXiv preprint arXiv:2503.06923*, 2025b. 1, 3, 5, 7

Xinyin Ma, Gongfan Fang, and Xinchao Wang. Deepcache: Accelerating diffusion models for free. In *Proceedings of the IEEE/CVF conference on computer vision and pattern recognition*, pp. 15762–15772, 2024. 3

Maxim Milakov and Natalia Gimelshein. Online normalizer calculation for softmax. *arXiv preprint arXiv:1805.02867*, 2018. 3

William Peebles and Saining Xie. Scalable diffusion models with transformers. In *Proceedings of the IEEE/CVF international conference on computer vision*, pp. 4195–4205, 2023. 1, 2

Pratheba Selvaraju, Tianyu Ding, Tianyi Chen, Ilya Zharkov, and Luming Liang. Fora: Fast-forward caching in diffusion transformer acceleration. *arXiv preprint arXiv:2407.01425*, 2024. 1, 3, 7

Junhyuk So, Jungwon Lee, and Eunhyeok Park. Frdiff: Feature reuse for universal training-free acceleration of diffusion models, 2024b. URL <https://arxiv.org/abs/2312.03517>, 2024. 3

Xingwu Sun, Yanfeng Chen, Yiqing Huang, Ruobing Xie, Jiaqi Zhu, Kai Zhang, Shuaipeng Li, Zhen Yang, Jonny Han, Xiaobo Shu, et al. Hunyuan-large: An open-source moe model with 52 billion activated parameters by tencent. *arXiv preprint arXiv:2411.02265*, 2024. 3

Genmo Team. Mochi 1. <https://github.com/genmoai/models>, 2024. 3

Jianyi Wang, Kelvin CK Chan, and Chen Change Loy. Exploring clip for assessing the look and feel of images. In *Proceedings of the AAAI conference on artificial intelligence*, volume 37, pp. 2555–2563, 2023. 7

Zhou Wang, Alan C Bovik, Hamid R Sheikh, and Eero P Simoncelli. Image quality assessment: from error visibility to structural similarity. *IEEE transactions on image processing*, 13(4):600–612, 2004. 7

Felix Wimbauer, Bichen Wu, Edgar Schoenfeld, Xiaoliang Dai, Ji Hou, Zijian He, Artsiom Sanakoyeu, Peizhao Zhang, Sam Tsai, Jonas Kohler, et al. Cache me if you can: Accelerating diffusion models through block caching. In *Proceedings of the IEEE/CVF Conference on Computer Vision and Pattern Recognition*, pp. 6211–6220, 2024. 3

Haocheng Xi, Shuo Yang, Yilong Zhao, Chenfeng Xu, Muyang Li, Xiuyu Li, Yujun Lin, Han Cai, Jintao Zhang, Dacheng Li, et al. Sparse video-gen: Accelerating video diffusion transformers with spatial-temporal sparsity. In *Forty-second International Conference on Machine Learning*, 2025. 1

Yifei Xia, Suhan Ling, Fangcheng Fu, Yujie Wang, Huixia Li, Xuefeng Xiao, and Bin Cui. Training-free and adaptive sparse attention for efficient long video generation. *arXiv preprint arXiv:2502.21079*, 2025. 1

Guangxuan Xiao, Yuandong Tian, Beidi Chen, Song Han, and Mike Lewis. Efficient streaming language models with attention sinks. *arXiv preprint arXiv:2309.17453*, 2023. 3

Ruyi Xu, Guangxuan Xiao, Haofeng Huang, Junxian Guo, and Song Han. Xattention: Block sparse attention with antidiagonal scoring. *arXiv preprint arXiv:2503.16428*, 2025. 1, 3

Shuo Yang, Haocheng Xi, Yilong Zhao, Muyang Li, Jintao Zhang, Han Cai, Yujun Lin, Xiuyu Li, Chenfeng Xu, Kelly Peng, et al. Sparse videogen2: Accelerate video generation with sparse attention via semantic-aware permutation. *arXiv preprint arXiv:2505.18875*, 2025. 1, 3

Zhuoyi Yang, Jiayan Teng, Wendi Zheng, Ming Ding, Shiyu Huang, Jiazheng Xu, Yuanming Yang, Wenyi Hong, Xiaohan Zhang, Guanyu Feng, et al. Cogvideox: Text-to-video diffusion models with an expert transformer. *arXiv preprint arXiv:2408.06072*, 2024. 3

Zihao Ye, Lequn Chen, Ruihang Lai, Wuwei Lin, Yineng Zhang, Stephanie Wang, Tianqi Chen, Baris Kasikci, Vinod Grover, Arvind Krishnamurthy, et al. Flashinfer: Efficient and customizable attention engine for llm inference serving. *arXiv preprint arXiv:2501.01005*, 2025. 8

Zhihang Yuan, Hanling Zhang, Lu Pu, Xuefei Ning, Linfeng Zhang, Tianchen Zhao, Shengen Yan, Guohao Dai, and Yu Wang. Ditfastatttn: Attention compression for diffusion transformer models. *Advances in Neural Information Processing Systems*, 37:1196–1219, 2024. 1, 3

Hanling Zhang, Rundong Su, Zhihang Yuan, Pengtao Chen, Mingzhu Shen Yibo Fan, Shengen Yan, Guohao Dai, and Yu Wang. Ditfastatttnv2: Head-wise attention compression for multi-modality diffusion transformers. *arXiv preprint arXiv:2503.22796*, 2025a. 1, 3, 7

Jintao Zhang, Chendong Xiang, Haofeng Huang, Haocheng Xi, Jun Zhu, Jianfei Chen, et al. Spageattention: Accurate and training-free sparse attention accelerating any model inference. In *Forty-second International Conference on Machine Learning*, 2025b. 1, 3, 5, 7

Richard Zhang, Phillip Isola, Alexei A Efros, Eli Shechtman, and Oliver Wang. The unreasonable effectiveness of deep features as a perceptual metric. In *Proceedings of the IEEE conference on computer vision and pattern recognition*, pp. 586–595, 2018. 7

Zhenyu Zhang, Ying Sheng, Tianyi Zhou, Tianlong Chen, Lianmin Zheng, Ruisi Cai, Zhao Song, Yuandong Tian, Christopher Ré, Clark Barrett, et al. H2o: Heavy-hitter oracle for efficient generative inference of large language models. *Advances in Neural Information Processing Systems*, 36:34661–34710, 2023. 3

Zangwei Zheng, Xiangyu Peng, Tianji Yang, Chenhui Shen, Shenggui Li, Hongxin Liu, Yukun Zhou, Tianyi Li, and Yang You. Open-sora: Democratizing efficient video production for all. *arXiv preprint arXiv:2412.20404*, 2024. 2

Chang Zou, Evelyn Zhang, Runlin Guo, Haohang Xu, Conghui He, Xuming Hu, and Linfeng Zhang. Accelerating diffusion transformers with dual feature caching. *arXiv preprint arXiv:2412.18911*, 2024. 1, 3

Chang Zou, Xuyang Liu, Ting Liu, Siteng Huang, and Linfeng Zhang. Accelerating diffusion transformers with token-wise feature caching. In *The Thirteenth International Conference on Learning Representations*, 2025. 1, 3, 7

A APPENDIX

A.1 EXPERIMENTAL DETAILS

A.1.1 SETUP

As is metioned in 4.1, the configuration for FlashOmni is specified as $(\tau_q, \tau_{kv}, \mathcal{N}, \mathcal{D}, S_q)$. In Table 4, we give details about them.

Settings	Description
τ_q	Sparsity threshold for q . Details: the importance scores of tokens are sorted in ascending order, and tokens are progressively marked for sparsification until the cumulative importance of the selected tokens exceeds τ_q .
τ_{kv}	Sparsity threshold for kv . Details: the importance scores of blocks are sorted in ascending order, and blocks are progressively marked for sparsification until the cumulative importance of the selected blocks exceeds τ_{kv} .
\mathcal{N}	Moderate cache interval.
\mathcal{D}	Order of expansion.
S_q	Threshold of caching. Details: if the proportion of tokens requiring computation is below this threshold, the layer degenerates into feature caching.

Table 4: Settings and their descriptions.

It is worth noting that the values of τ_q and τ_{kv} are not set to their target values at the initial time step. Rather, they progressively converge to these values as the time step advances.

We conducted experiments on three models for different tasks: FLUX for the text-to-image generator, HunyuanVideo for the text-to-video generator, and FLUX.1-Kontext for text-guided image editing. We selected five representative parameters for evaluation, including τ_q at 5% and 50%; τ_{kv} at 15%, \mathcal{N} of 3, 4, 5, 6, and 7; \mathcal{D} of 0, 1, and 2; S_q at 0% and 30%. Our experiments achieved excellent results, maintaining high generation quality even under high sparsity levels. It is worth noting that these parameters can be efficiently tuned via lightweight search algorithms to further enhance the performance of FlashOmni. We plan to implement this optimization in future work.

A.1.2 GEMM- O SPEEDUP METRICS

In this section, we define our methodology for computing the speedup metric of GEMM- O . Define T_{total} as the total time taken to execute a single $\text{Proj}_{\text{to_out}}$ operation and s to denote the sparsity ratio, then we can compute the normal time consumption: $\mathcal{N}T_{total}$, and the FlashOmni time consumption:

$$\begin{aligned}
 T_{\text{FlashOmni}} &= T_{\text{sparse}} + T_{\text{computation}} \\
 &= T_{\text{total}} \times s + \sum_{\mathcal{N}} ((1 - s) \times T_{\text{total}}) \\
 &= T_{\text{total}} + (\mathcal{N} - 1)(1 - s)T_{\text{total}}
 \end{aligned} \tag{5}$$

Then we can compute the speedup metric $\frac{N}{1 + (N-1)(1-s)}$. When the $s = 0.9$ and $\mathcal{N} = 6$, the theoretical speedup is $\frac{6}{1 + (6-1)(1-0.9)} = 4$. As is shown in Figure 6, our actual speedup obtained under this configuration is $3.509 \times$, approaching the theoretical value of $4 \times$, which substantiates the high efficiency of FlashOmni.

A.1.3 WARMUP STEPS ANALYSIS FOR FLUX

Figure 9 shows the end-to-end metrics comparison with feature caching on FLUX with different warmup steps. It is evident that when the warmup step count is low, the TaylorSeer method experiences a significant drop in image quality, with poor performance across PSNR, LPIPS, SSIM, and FID metrics, indicating a strong dependence on a high number of warmup steps. In contrast, while the FlashOmni method also shows a decline in quality at lower warmup steps, it still maintains relatively high generation quality and does not require a large warmup step count to achieve satisfactory results.

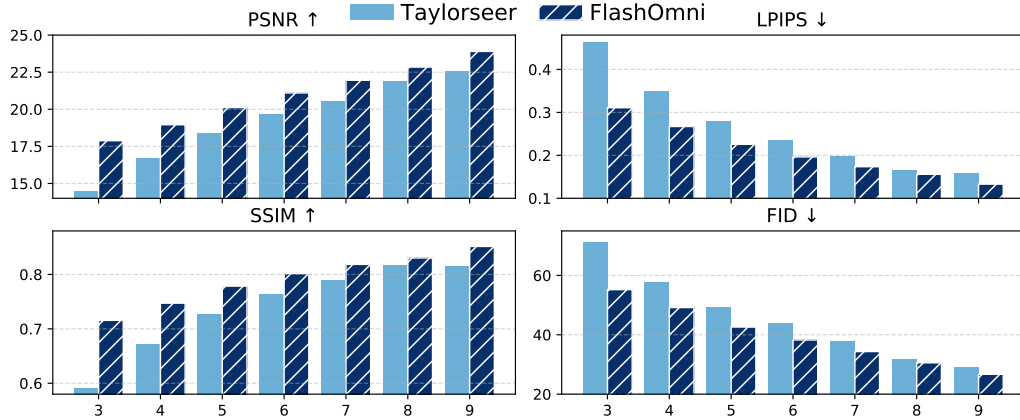


Figure 9: End-to-end metrics comparison with feature caching on FLUX with different warmup steps.

Table 5: End-to-end metrics comparison on text-guided image editing model.

Method FLUX.1-Kontext	Configuration	PSNR (\uparrow)	LPIPS (\downarrow)	SSIM \uparrow	FID (\downarrow)
Full-Attention	50 steps	∞	—	—	—
DiTFastAttnV2	$(\theta = 0.2)$	24.507	0.1233	0.8225	37.232
SpARGEAttn	$(l_1 = 6\%, l_2 = 6.5\%)$	26.851	0.1048	0.8519	28.163
FlashOmni	$(50\%, 15\%, 5, 1, 0)$	31.590	0.0466	0.9201	13.218
TaylorSeer	$(\mathcal{N} = 5, \mathcal{D} = 1)$	29.733	0.062	0.8919	15.876
FlashOmni	$(50\%, 15\%, 5, 1, 20\%)$	30.689	0.0543	0.9082	15.204

A.1.4 SUPPLEMENTARY FLUX.1-KONTEXT RESULTS

Table 5 complements the evaluation by providing an end-to-end metrics comparison on a text-guided image editing model. The results demonstrate the superior performance of FlashOmni in the FLUX.1-Kontext setting for text-guided image editing.

A.2 FLASHOMNI ATTENTION

We evaluate the inference performance of the attention kernel under different sparsity levels during high-resolution diffusion, including 2K image generation in Flux, video generation in HunyuanVideo, using token lengths of 17K and 33K as examples. Three configurations are tested: activating only FC, activating only BSS, and activating both. All sparse symbols are randomly generated, with the random seeds for BSS varying across groups. @1, @2, and @3 correspond to BSS sparsity thresholds of 0.1, 0.3, and 0.5, respectively, while, within each group, the FC threshold increases incrementally (0.1, 0.2, 0.4, 0.6, 0.8). Our experiments show that, at the same sparsity level, FC achieves higher speedup than BSS. This is because FC requires only a single decoding operation on the CUDA cores, whereas BSS—despite having the same sparsity—requires multiple decoding operations along the reduction axis, which reduces efficiency. For the combined sparsity strategy, the speedup scales almost linearly with sparsity (approximately a 1:1 ratio). As an illustration, a combined sparsity of 90% yields an observed speedup of about $\sim 9.4\times$ in Figure 10.

A.3 FLASHOMNI SPARSE GEMM- O

We further evaluated the GEMM- O speedup performance across three representative resolution settings for the generation tasks. As shown in the Figure 11, for tasks at standard resolutions (e.g., 1K image generation in FLUX.1), the parallelism of the kernel is relatively limited, and the influence of CUDA Core decoding operations becomes higher. Consequently, the speedup is lower compared to the ultra-high-resolution scenarios. Nevertheless, the acceleration remains notable, achieving approximately $2.5\times$ – $3.4\times$ speedup across different \mathcal{N} settings. In the ultra-high-resolution cases, the speedup increases further, reaching avg $2.7\times$ – $3.9\times$.

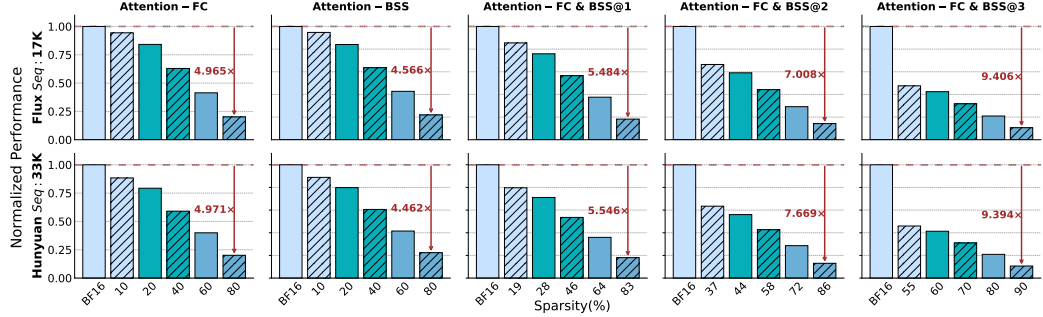


Figure 10: Normalized inference performance on NVIDIA A100 (BF16, measured by using FlashInfer) at different sparsity levels for sparse attention kernels. FC and BSS indicate the application of feature caching and block-sparse skipping, respectively.

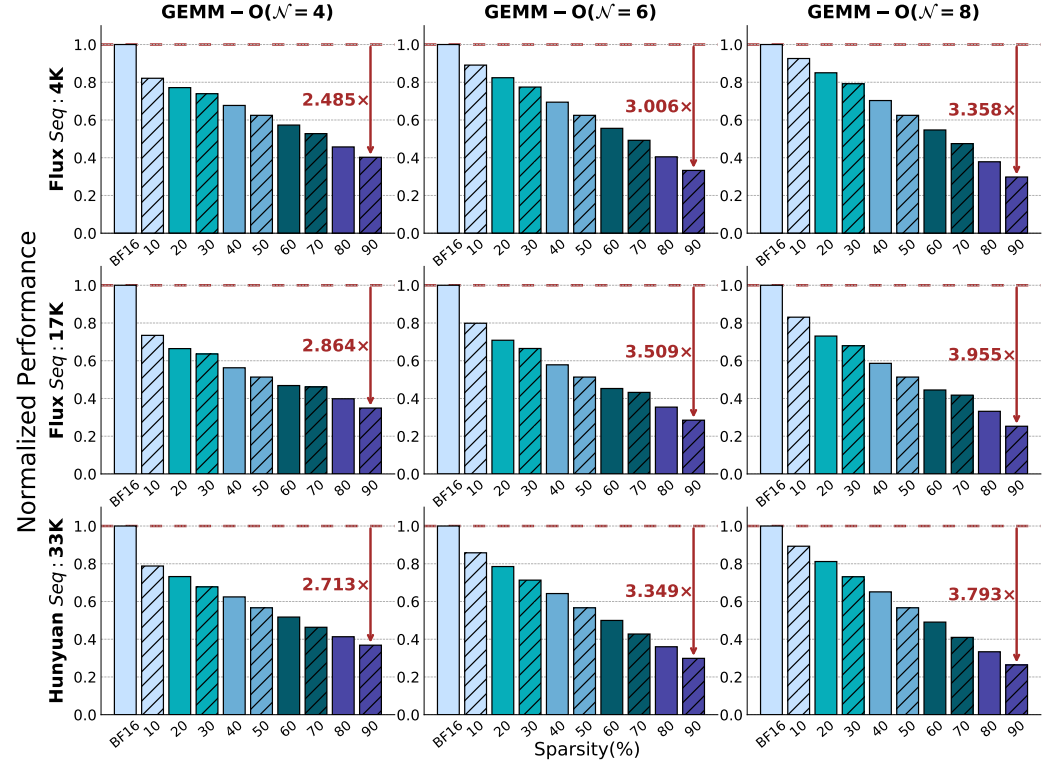


Figure 11: Normalized inference performance on NVIDIA A100 (BF16, measured by using cudaLib) at different sparsity levels for sparse GEMM- O , whose N includes 4,6,8.

A.4 FLASHOMNI PROGRAMMING INTERFACE

```

import flashomni

# Attention Processor Modules
def __attn_wrapper__(self = AttnProcessor, task_info):
    self.attn_proc = flashomni.AttentionWrapper(task_info)

def __call__(self = AttnProcessor, attn, x, cache_dic):
    q = flashomni.to_q(cache_dic.sparse_symbols, x)                                # FlashOmni GEMM Q
    ...
    attn_out = self.attn_proc(q,k,v, cache_dic.sparse_symbols)                      # FlashOmni Attention
    ...
    if cache_dic[type] == "update":
        # FlashOmni Sparse Symbols
        cache_dic.sparse_symbols = self.update_sparse_symbols(q, k)
        # Cache bias generation
        cached_bias = flashomni.to_out(attn_out, cache_dic.sparse_symbols)           # FlashOmni GEMM O
    out = flashomni.to_out(attn_out, cache_dic.sparse_symbols, cached_bias)          # FlashOmni GEMM O
    return out

```

A.5 SUPPLEMENTARY VISUALIZATION RESULTS

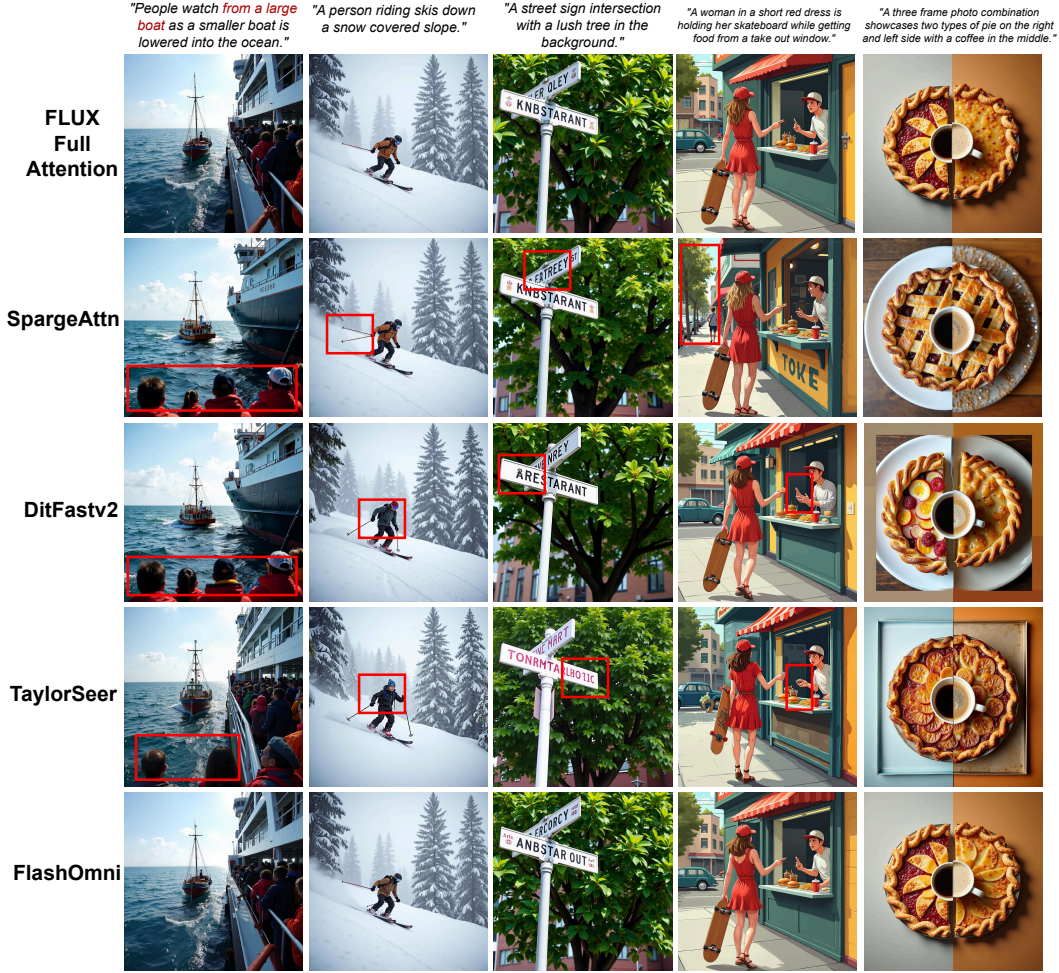


Figure 12: Visualization results for different acceleration methods on FLUX.1-dev.



Figure 13: Visualization results for different acceleration methods on Hunyan Video.